Multi-stiffness topology optimization of zero Poisson's ratio cellular structures

Jian Huang[a,c], Qiuhua Zhang[a], Fabrizio Scarpa[b,*], Yanju Liu[a], Jinsong Leng[c,**]

[a] Department of Aerospace Science and Mechanics, No. 92 West Dazhi Street, Harbin Institute of Technology (HIT), P.O. Box 301, Harbin 150080, PR China
[b] Bristol Composites Institute (ACCIS), University of Bristol, BS8 1TR, UK
[c] Center for Composite Materials and Structures, No. 2 Yikuang Street, Science Park of Harbin Institute of Technology (HIT), P.O. Box 301, Harbin, PR China

ARTICLE INFO

ABSTRACT

This work features a multi-stiffness topology optimization of a zero Poisson's ratio cellular structure for morphing skin applications. The optimization is performed with stiffness constraints to minimize the weight by using a state-of-the-art solid isotropic microstructure with penalty (SIMP) method. The topology optimization has been performed to minimize flatwise compressive and transverse shear moduli for aerodynamic pressures and shear forces. The multi-stiffness topology optimization is performed using a norm method with weighting coefficients. Both the single-stiffness and the multi-stiffness topology optimization have generated new honeycomb design by imposing symmetry conditions and geometric post-processing to avoid the presence of stress concentrations. The mechanical performances of the new honeycomb designs are validated using two approaches: one based on force boundary conditions (HyperWorks) and another with displacement BCs (ANSYS). The work shows some alternate potential topologies and configurations of cellular structures for lightweight zero Poisson's ratio honeycomb designs.

1. Introduction

Honeycomb structures have been widely used in applications ranging from marine to aerospace and automotive for their outstanding lightweight and tailorable design mechanical performances [1,2]. The mechanical performances of honeycomb structures are directly dependent on their topological configurations and core material properties. The conventional hexagonal honeycomb structure is a typical example of a cellular configuration that exhibits in-plane positive Poisson's ratio (PPR) [1]. Recent work performed on hexagonal cellular configurations has however further developed the functionality of this particular lattice topology. Liu et al. have proposed and developed a three-dimensional unit cell model for the flatwise compressive properties of Nomex hexagonal honeycomb cores with debonding imperfections in the double cell walls [3]. Sun et al. have investigated the compressive properties of composite sandwich structures with periodical grids reinforced hexagonal honeycomb cores [4]. Wang et al. have also discussed the mechanical behaviors of inclined cell honeycomb structures under our-of-plane compressive loading through experiments and finite element simulations [5]. Tao et al. have proposed a novel in-plane graded honeycomb structure by introducing gradient into hexagonal

cellular materials, and studied its dynamic behavior when subjected to out-of-plane compression using numerical simulation and theoretical analysis [6]. Choi et al. have designed a novel broadband microwave-absorbing hexagonal honeycomb structure produced with a lossy electromagnetic material [7]. Honeycomb structures with PPR show anticlastic or saddle-shaped curvatures when subjected to out-of-plane bending deformation [8,9]. On the contrary, if the in-plane Poisson's ratio of the honeycomb structures is negative as in the re-entrant hexagonal [1,10,11], hexachiral [12–15], and anti-tetrachiral honeycombs [16,17], the curvatures are synclastic and result in a dome-shaped bent structure [13,18]. Honeycombs with negative Poisson's ratio (NPR) are also described as auxetic [19–21]. Compared with conventional hexagonal honeycombs, the auxetic configurations feature compliant in-plane shear and enhanced indentation resistance [9,19,22]. Subramani et al. have developed novel auxetic structures from braided composites using the re-entrant hexagonal cellular structure [23]. Jin et al. have proposed an innovative sandwich structure with re-entrant hexagonal cell cores [24]. Its dynamic performance and blast resistance under explosion loading have been investigated numerically. Hou et al. have described experimental tests of graded conventional/auxetic honeycomb cores manufactured using Kevlar woven fabric/914 epoxy

---

* Corresponding author.
** Corresponding author.
  E-mail addresses: f.scarpa@bristol.ac.uk (F. Scarpa), lengjs@hit.edu.cn (J. Leng).

prepreg under flatwise compression and edgewise loading [25]. The effect of translational disorder on hexachiral honeycombs has also been investigated through a finite element approach [26]. The bending performances of the honeycomb structures with PPR or NPR however limit their applications in cylindrical bending morphing engineering [27]. Cellular structures with zero Poisson's ratio (ZPR) like the SILI-COMB [28–30], chevron [31–33], and accordion [34] however feature no synclastic or anticlastic curvature when bent out-of-plane. ZPR also implies that the solids exhibit no lateral deformations when subject to uniaxial tensile or compressive loading. The two special properties make cellular structures with ZPR performance more suitable for cylindrical or one-dimensional morphing applications [31,35]. Honeycomb structures have recently been proposed as a promising solution for morphing skins, which is a critical technology for the design of morphing aircrafts [36,37]. Honeycomb structures with ZPR performance have been also applied in biomedical scaffolds [38], and one-dimensional spanwise morphing flexible skins [34,36]. To increase the bending flexibility of all the forementioned cellular structures the flatwise compressive and the transverse shear stiffness will inevitably decrease, because the minimization of cell walls thickness and the maximization of the unit cell size are the only two ways to achieve the objective in periodic regular monomaterial structures. Special attention should be paid to novel ZPR and NPR honeycomb structures that can achieve uncoupled in-plane and out-of-plane mechanical performances by tessellation of thin plates and hexagons within the cells [39–42].

In this work we present the result of a multi-stiffness topology optimization of zero Poisson's ratio honeycomb structures to minimize the weight with stiffness constraints for morphing skin applications using the solid isotropic microstructure with penalty (SIMP) method. Topology optimization (TO) has been previously applied to design auxetic cellular structures with enhanced vibration damping behavior [43], and other transverse auxetic core for flat sandwich panels [44]. As far as the authors know this is the however the first targeted on the light weight design of honeycomb morphing structures using topology optimization technology. Honeycomb configurations used in morphing skins as supporting structures not only bear the aerodynamic pressure, but also aerodynamic-induced shear forces. We perform a lighter weight design of the original ZPR morphing honeycomb configurations against the flatwise compressive stiffness and the two transverse shear stiffness values. Firstly, the single-stiffness topology optimization is performed separately against the three engineering constants to obtain the possible minimal weights under only one corresponding stiffness constraint. A multi-stiffness topology optimization is then carried out using a norm method with weighting coefficients. From these optimization processes we propose new morphing honeycomb designs. The out-of-plane performances of the new designs have also been validated using two Finite Element approaches: an analysis with force boundary conditions (performed with HyperWorks) and one based with displacement boundary conditions (ANSYS commercial software).

2. Basic theory of the topology optimization method

Structural optimization can be divided into three levels-topology, shape and size optimizations, corresponding to the conceptual, preliminary and detailed design periods during the structural design process [45] (Fig. 1). The topology of a structure crucial for its optimality can be interpreted as an arrangement of materials in the structure [45]. The topology optimization is performed at a very early stage of the design process, and aims to find the very best possible configuration from a weight reduction point of view, which is generally the most critical factor of the structure efficiency. The shape and size optimization do not provide any global change to the topology of a structure when finding the characteristic optimal solutions. Therefore, the value of the topology optimization lies in providing the optimal arrangement of materials in the preprocessing of the shape and size optimization [46,47].
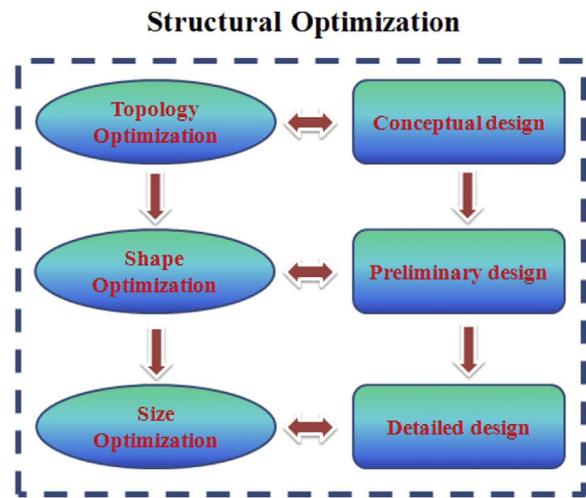

Fig. 1. Optimization methods for different structural design stages.

The homogenization approach used to solve topology optimization problems of continuum structures was first proposed by Bendsøe and Kikuchi [48] in 1988. The homogenization method optimizes the structural performances in terms of density variables, but the mathematical complexity of this approach prevents its general application. A year later, Bendsøe [49] proposed another density-based technique known as the variable density method (VDM), by using the much simplified assumption that the stiffness of the material is linearly dependent on its density. Since then, VDM has been widely used and often integrated with the finite element method (FEM). In VDM, the material density of each element is used as the design variable and always varies continuously between 0 and 1. In this case 0 represents the void, 1 represents the solid, and the values between 0 and 1 represent fictitious materials that are impractical when determining the topology of the structure in the design domain. Hence, the VDM with penalty factor forces the final design density of the material to be approximately either 0 or 1 (solid isotropic microstructure with penalty (SIMP) [50,51]). For two-dimensional or three dimensional solid elements, the SIMP method can be expressed as following,

$$K'_{(\rho)} = \rho^P \times K \qquad (1)$$

In (1) ρ is the relative density of the solid element and K' and K represent the penalized and the real stiffness matrix, respectively. P is the penalty factor, always larger than 1. As shown in Fig. 2, a larger penalty factor leads to a more discrete result. Because of its simplicity in conception, assumption and numerical implementation, the SIMP method has become the most popular and successful approach in
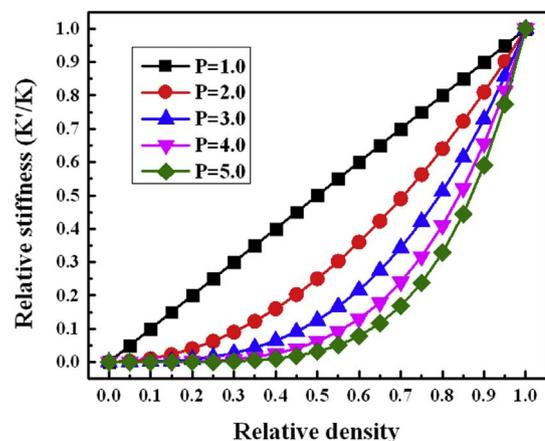

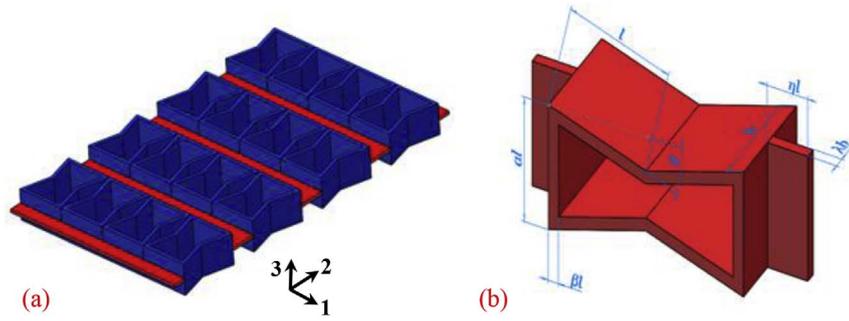**Fig. 2.** Schematic graph of the SIMP method with varying penalization factors.

structural topology optimization. There are however several alternative methods proposed, such as the evolutionary structural optimization (ESO) developed by Xie and Steven [52], the level-set [53–55], the phase filed [56], bubble [57], and the topological derivative methods [58].

3. Model demonstrations

3.1. Geometry of the unit cell

The zero Poisson's ratio cellular structures consist of two parts that provide tailorable mechanical performances: one is a re-entrant hexagonal structure that provides the out-of-plane compressive stiffness and in-plane compliance, the other one is the thin plates connecting the re-entrant hexagons and providing large out-of-plane flexibility (Fig. 3) [39,41]. The unit cell is composed of four inclined walls with same length l and tilt angle θ, two vertical walls equal length $h = \alpha l$, and two thin plates located in the middle of the re-entrant hexagon along the thickness direction. All the inclined and vertical walls have a same thickness represented by the parameter βl. The thickness of the unit cell along the 3-direction is represented by the parameter b. The two thin plates have same dimensions ηl, thickness λb and width equal to the length of the vertical walls. In these simulations we use parameters with value of $l = 10\,\text{mm}$, $\theta = 15°$, $\alpha = 1.5$, $\beta = 0.1$, $b = 10\,\text{mm}$, $\eta = 0.3$, $\lambda = 0.1$. The isotropic material properties of the core are $E_s = 2129\,\text{MPa}$ and $\nu_s = 0.42$ [39].

3.2. The finite element model and the equivalent stiffness

The commercial finite element software HyperWorks (Version 12.0, Altair Engineering, Inc.) has been used in the topology optimization process, and the finite element model of a unit cell is shown in Fig. 4. To ensure the continuity of the optimized results, the unit cell has been split up into two sections: the design domain and the non-design
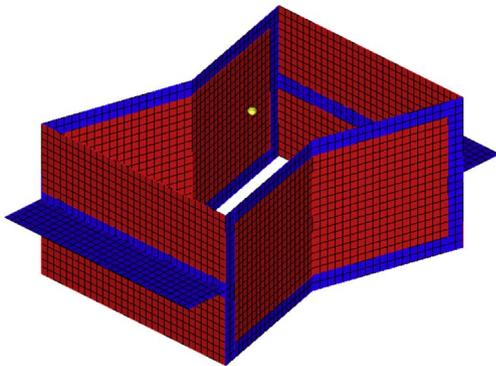

Fig. 4. The FE model used in the topology optimization process with the design domain (red), the non-design domain (blue) and a master node on the top surface. (For interpretation of the references to colour in this figure legend, the reader is referred to the Web version of this article.)

domain, with only the design domain been set as the design variable. The volume fraction of the design domain is 70.63%. The unit cell has been meshed using the property of P-SHELL with quads only mesh type and an element size of $l/20$. A master node has also been created at the center of the top surface. All the nodes located on the top surface have been coupled with the master node with a rigid element RBE2 to simulate the mechanical boundary conditions typical of the skin/core interface interaction in sandwich structures. All the translational and rotational degrees of the nodes on the bottom surface have been fixed (clamped). To consider the interaction among the unit cells into account, anti-symmetric boundary conditions have been applied on the six free edges of the two thin plates [59]. To allow for some control over the member size of the final topology and the simplicity of the final design, all the topology optimization in this work has been however carried out using a minimum member size control of $l/10$. When the minimum member size control is used, the penalty factor starts at 2 and then increases to 3 during the second and third iterative phases to obtain a more discrete result [HyperWorks 12.0 help]. To calculate the flatwise compressive modulus E_3 and the two transverse shear modulus G_{13} and G_{23}, three forces of $F_3 = 1000\text{N}$, $F_1 = 1000\text{N}$, $F_2 = 1000\text{N}$ have been loaded on the master node for the three cases respectively. The equivalent stiffness of the out-of-plane mechanical performance of the unit cell can be calculated by using the following expressions:

$$E_3 = \frac{\sigma_3}{\varepsilon_3} = \frac{F_3}{(2\eta l + 2l\cos\theta)\beta l} \Big/ \left(\frac{\delta_{33}}{b}\right)$$
$$G_{13} = \frac{\tau_{13}}{\gamma_{13}} = \frac{F_1}{(2\eta l + 2l\cos\theta)\beta l} \Big/ \left(\frac{\delta_{13}}{b}\right)$$
$$G_{23} = \frac{\tau_{23}}{\gamma_{23}} = \frac{F_2}{(2\eta l + 2l\cos\theta)\beta l} \Big/ \left(\frac{\delta_{23}}{b}\right) \tag{2}$$

In (2) the parameters δ_{33}, δ_{13}, δ_{23} represent the corresponding displacements of the master node along the 3-, 1-, 2-directions of the three loading cases respectively. The ZPR behavior of the cellular structure is caused by the presence of the thin plates [39,41]; in this work those plates belong to the non-design domain, and one can therefore infer that the ZPR performance of optimized results is not affected by the topology optimization process.

4. Single-stiffness topology optimization

The single-stiffness topology optimization has been done using the following model:

Find: $\overline{\rho} = (\rho_1, \rho_2, ..., \rho_n, ..., \rho_{n_d})$, $0 < \rho_n \leq 1$, $n = 1, 2, ..., n_d$

Minize: $V_{ij}(\overline{\rho})$

Subject to: $E_{ij} \geq E_{ij0}/m$ $\tag{3}$

In (3) ρ_n is the pseudo-density variable describing a void or a solid finite element when it is 0 or 1; n_d is the number of density variables, while $m > 1$ is a coefficient determining the stiffness constraints. The design objectives consist in minimizing the volume fraction of the zero Poisson's ratio honeycomb structure separately, according to the three out-of-plane mechanical engineering constants. As the honeycomb structure is made by using one isotropic material phase only, to
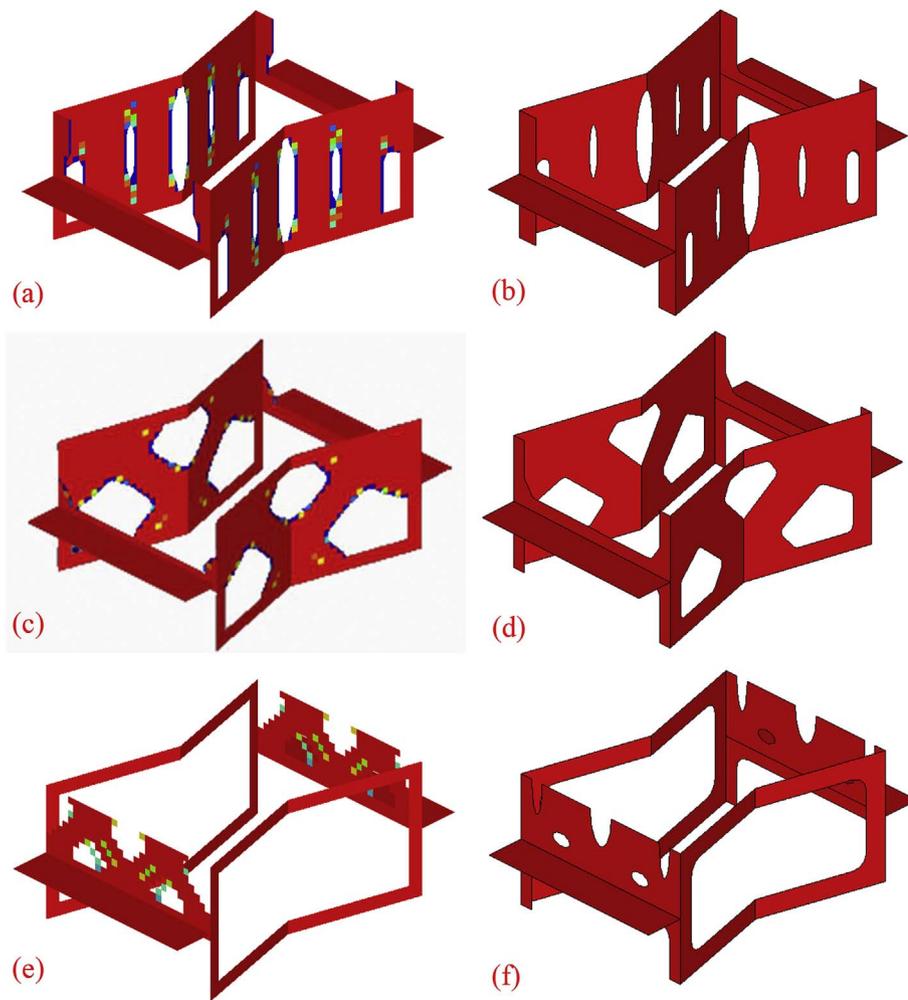
minimize its volume fraction implies the minimization of its weight. As minimizing the volume fraction will inevitably decrease the mechanical performances of the honeycomb structure, we have set half of the original values of the stiffness ($m = 2$) as the lower limit of the constraints, to make sure the optimized structure still retains some stiffness. According to equation (2), the constraints of this single-stiffness topology optimization have been obtained by applying the displacements of the master node for varying load steps under different boundary conditions.

4.1. Results of the single-stiffness topology optimization

The results of the topology optimization using the solid isotropic microstructure with penalty (SIMP) method are usually expressed by the relative density of every element not only in the design domain but also in the non-design domain. Therefore, elements with low relative density ($\rho < 0.3$) have been artificially removed to provide a clear shape of the optimized topology of the structure (Fig. 5). In this section, the coefficient m in equation (3) has been set as 2. From the results of the single-stiffness topology optimization, it is possible to appreciate the necessity to divide the unit cell into design and non-design domains in order to keep the connectivity of the topology. As shown in Fig. 5, the vertical walls are not necessary to maintain the flatwise compressive stiffness (modulus E_3) and transverse shear (modulus G_{13}). The vertical walls are however critical for the transverse shear load capability (modulus G_{23}). The inclined walls play on the opposite some a very important role to ensure the flatwise and traverse shear stiffness in the 13 plane, but they offer little load bearing capability for the transverse

shear in the 23 plane. For single-stiffness topology optimization the new honeycomb designs shown in Fig. 5 have been obtained by edge smoothing and by transforming into symmetric areas the voids, to prevent stress concentration. Also, elements with relative density between 0.3 and 1 have been artificially changed into solid ones.

4.2. Stiffness validation of the new designs

The validation of the out-of-plane mechanical performances of the new designs following the single-stiffness topology optimization has been performed in two ways: the first is by using the HyperWorks code with force boundary conditions, and the second using ANSYS (Version 13.0, ANSYS Inc.) with displacement BCs. After convergence tests, the finite element models of the new designs (shown in Fig. 6) used in the HyperWorks and ANSYS analyses have been freely meshed with an element size of 20/l because of the irregular geometry. The elements used were both quadrilateral with 4 nodes with 6° of freedom (P-SHELL and the SHELL 181 in HyperWorks and ANSYS analyses respectively). The boundary conditions of the HyperWorks simulations are the same used for the topology optimization (Section 3.2) and the results are also calculated using equation (2). The ANSYS analyses are performed using the displacement boundary conditions following [59], because of the convenience of using the internal APDL language to obtain the corresponding average stresses. In all three loading cases all the degrees of freedom of the nodes at the bottom surface are constrained, while the nodes at the six free edges of the end thin plates are loaded with antisymmetric boundary conditions to consider the periodicity of the unit cells layout. All the nodes on the top surface are loaded with one of the
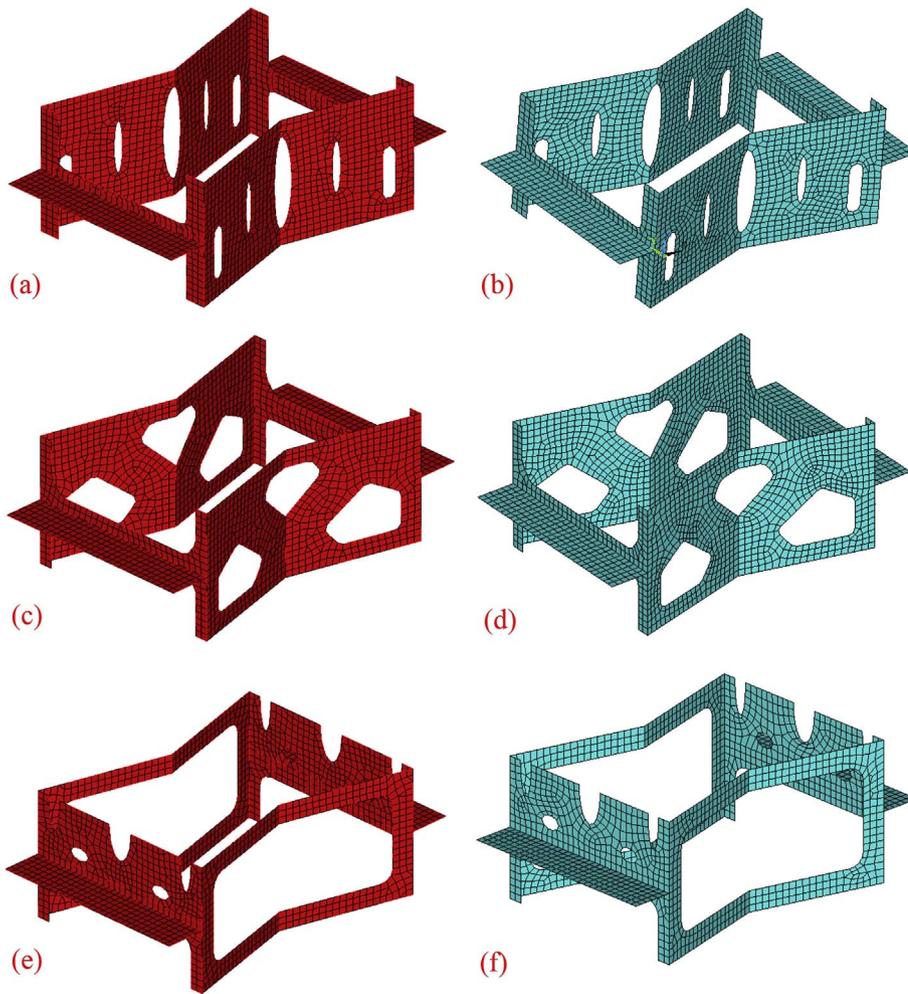
Fig. 6. Finite element models of the HyperWorks (red) and ANSYS (blue) analyses used to validate the out-of-plane mechanical performances of the new designs: (a) and (b), flatwise compressive modulus E_3; (c) and (d), transverse shear modulus G_{13}; (e) and (f), transverse shear modulus G_{23}. (For interpretation of the references to colour in this figure legend, the reader is referred to the Web version of this article.)

three imposed displacements u_3, u_1, u_2, according to the three cases of E_3, G_{13} and G_{23} respectively. The average strains corresponding to the three loading cases are calculated using the ratios between the imposed displacements and the gauge thickness of the structure. The three out-of-plane moduli are obtained as the ratios between the average stresses and the imposed strains.

4.3. Results and discussions

The values of the out-of-plane mechanical performances and weight reduction of the new designs against the original ones are listed in Table 1. The values of the new designs from the displacement BCs analysis (ANSYS) show stiffer properties than the HyperWorks one for the engineering constants E_3, G_{13} and G_{23} (1.48%, 7.45% and 3.93% respectively). All the values of the new designs are 50% larger than the corresponding original design ones, which represent the lower limits of the stiffness constraint used in the topology optimization process. This phenomenon is induced by artificially changing the elements with

relative density between 0.3 and 1 into solid ones. Weight reductions of 30.13%, 38.13% and 45.57% are achieved for the three single-stiffness topology optimization cases.

To investigate the influence of the parameter m in the stiffness constraint, the single-stiffness topology optimizations have been repeated for varying $m = 1.2, 1.4, 1.6, 1.8, 2.0, 2.2, 2.4, 2.6, 2.8, 3.0$. The geometrical shapes of the optimized results are shown in Fig. 7. An increasing value of m leads to more material being removed in the design space. The variation of the volume fraction of the design space versus the stiffness constraint parameter m is shown in Fig. 8. Increasing values of m result in decreasing of the volume fraction, and the slope of the curves also decreases gradually. When m increases from 1.2 to 3.0, the volume fraction of the flatwise compression case is subjected to a large decrease from 82.50% to 23.44%. In other words, large weight reductions can be achieved under the design requirement for the flatwise compressive stiffness. For the other two transverse shear cases the volume fraction decreases from 50.18% to 37.22%–10.48% and 10.04% respectively when m increases from 1.2 to 3.0. Special attention should be paid to the two values of 50.18% and 37.22%, which represent the volume fraction for the transverse shear moduli G_{13} and G_{23} cases. The two transverse moduli decrease in this case to 5/6 of the original values. From observing Fig. 7 (b), one can also draw the conclusion that the vertical walls account little in the transverse stiffness, with a very little decrease of the G_{13} modulus resulting in a large amount of the material in the vertical walls being removed. The same phenomenon is also present for the inclined walls, this time for the G_{23} engineering constant.

Table 1
Stiffness and weight reduction of the new designs compared with the original design for the single-stiffness topology optimizations.

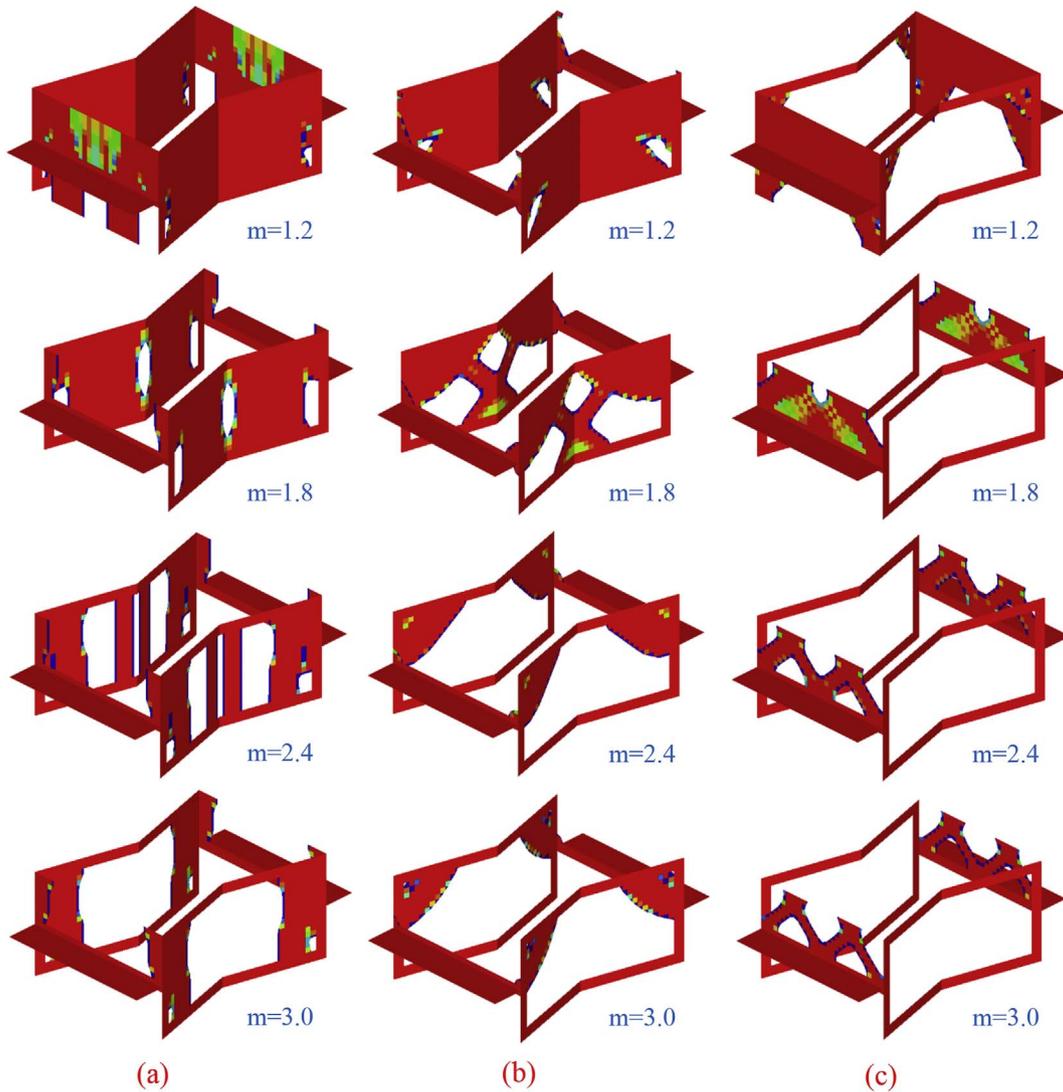| Stiffness (MPa)					Weight Reduction		
		E_3	G_{13}	G_{23}	E_3	G_{13}	G_{23}
Original	HyperWorks	487.61	95.23	87.67	30.13%	38.13%	45.57%
New	ANSYS	296.30	70.65	60.07			
	HyperWorks	291.92	65.75	57.80			

Fig. 7. Topology of the optimized results VS the constraint's parameter m: (a) flatwise compressive modulus E_3; (b) transverse shear modulus G_{13}; (c) transverse shear modulus G_{23}.
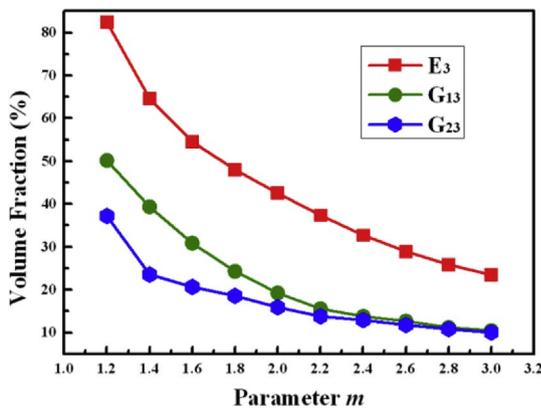

Fig. 8. vol fraction of the design domain for the optimized results VS the constraint's parameter m.

5. Multi-stiffness topology optimization

In real operational environments the morphing skins are loaded with a combination of all the aerodynamic compressive pressure and transverse shear forces, making therefore the multi-stiffness topology optimization of the zero Poisson's ratio honeycomb structure necessary

to meet the requirements of realistic loading conditions. In this work, we present a norm method with weighting coefficients [60–62] for the multi-stiffness topology optimization. The methodology can be expressed as follows:

Find: $\overline{\rho} = (\rho_1, \rho_2, ..., \rho_n, ..., \rho_{n_d})$, $0 < \rho_n \leq 1$, $n = 1,2,...,n_d$

Minize: $F(V)$

$$= \left[w_3 \left(\frac{V - V_{3\min}}{V_{\max} - V_{3\min}} \right)^2 + w_1 \left(\frac{V - V_{1\min}}{V_{\max} - V_{1\min}} \right)^2 + w_2 \left(\frac{V - V_{2\min}}{V_{\max} - V_{2\min}} \right)^2 \right]^{\frac{1}{2}}$$

Subject to: $\begin{cases} E_3 \geq E_{30}/m \\ G_{13} \geq G_{130}/n \\ G_{23} \geq G_{230}/k \end{cases}$

(4)

Where, V is the volume fraction of the current iterative, $V_{\max}$ the maximal volume fraction of the design domain, V_{3min}, V_{1min} and V_{2min} are the minimal volume fraction obtained from the single-stiffness topology optimization for the cases of E_3, G_{13} and G_{23} respectively. E_{30}, G_{130} and G_{230} are the values for the original design, while m, n, k are the coefficient for the stiffness constraints. The most important feature of for this methodology is the weighting coefficients w_3, w_1 and w_2, which are respectively corresponding to E_3, G_{13} and G_{23} under the condition $w_3 + w_1 + w_2 = 1$. In this section, $m = n = k = 2.0$, $w_3 = 0.4$, and $w_1 = w_2 = 0.3$ have been used for the topology optimization. For this multi-stiffness topology optimization the stiffness constraints are also
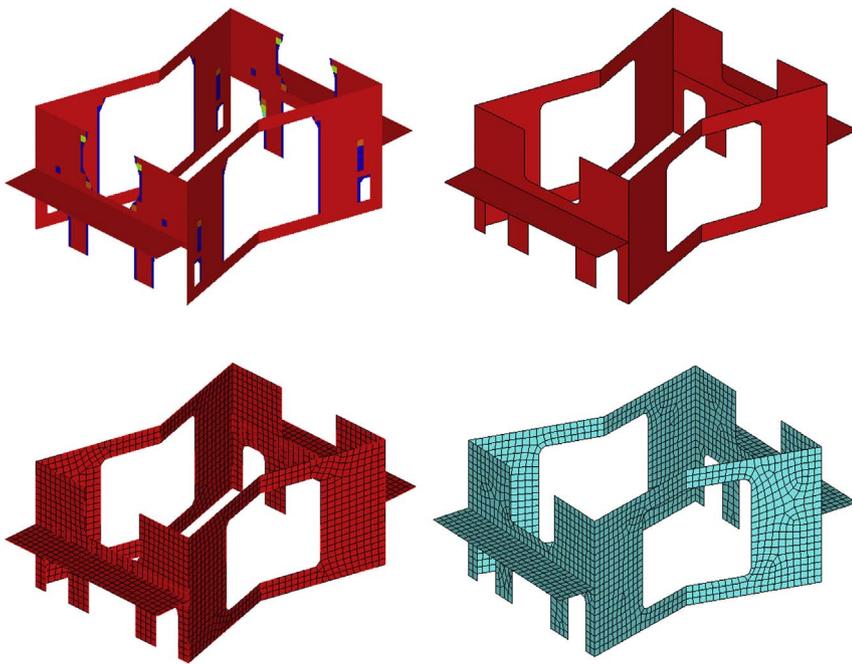
Fig. 9. Result of the multi-stiffness topology optimization with relative density ρ ≥ 0.3 (left) and the new design according to the optimized result (right).

Fig. 10. Finite element models of the HyperWorks (red) and ANSYS (blue) analyses used to validate the out-of-plane mechanical performances of the new design. (For interpretation of the references to colour in this figure legend, the reader is referred to the Web version of this article.)

been executed using the displacement of the master node for the different load steps.

5.1. Results and discussions

Result of the multi-stiffness topology optimization for the zero Poisson's ratio honeycomb structures are shown in Fig. 9. To assure the three out-of-plane engineering constants meeting the constraints, the elements in the design space of the vertical walls and the inclined walls are only partially removed. Like in the previous single optimization case, the new honeycomb design has been adjusted by imposing symmetric features and edge smoothing to avoid stress concentrations. Also in this case, elements with relative density ρ < 0.3 have been removed from the final configuration. To validate the out-of-plane mechanical performances of the new honeycomb design, force boundary conditions (Hyperworks) and displacement boundary conditions (ANSYS) have been used for the simulations. The HyperWorks and ANSYS calculations are performed following the same procedure used for the cases related to the single-stiffness topology optimization in Section 4.2 (see Fig. 10).

The out-of-plane mechanical performances of the new honeycomb design obtained from the HyperWorks and ANSYS analyses are listed in Table 2. For the new design the flatwise compressive modulus E_3 from the ANSYS analysis is 6.20% stiffer than the analogous value from the HyperWorks analysis. For the cases of the two transverse shear moduli HyperWorks gives however 6.81% and 8.11% larger values than the displacement BCs analysis. In any case the values obtained both from the HyperWorks and ANSYS analyses meet the requirement of the stiffness constraints used in the topology optimization when compared with the corresponding values of the original honeycomb configuration.

Table 2
Stiffness and weight reduction of the new design compared with the original design for the multi-stiffness topology optimization.

Stiffness (MPa)					Weight Reduction
		E_3	G_{13}	G_{23}	
Original	HyperWorks	487.61	95.23	87.67	31.77%
New	ANSYS	287.01	51.23	44.13	
	HyperWorks	270.26	54.72	47.71	

A weight reduction of 31.77% is been achieved by this multi-stiffness topology optimization procedure. To understand the influence of the weighting coefficients on the geometric shape of the result, a TO using varying weighting coefficients is been carried out and the results are shown in Fig. 11. When the three moduli make equal contributions to the optimized result (w_3 = 0.34, w_1 = w_2 = 0.33) and only the flatwise compressive modulus E_3 and the transverse shear modulus G_{23} are taken into account (w_3 = w_2 = 0.5, w_1 = 0), similar results as the one in Fig. 9 are obtained. Topology optimizations for other two groups of combinations of the weighting coefficients considering only two of the three mechanical moduli clearly show different geometric shapes (Fig. 11 (b) and (d)).

The cellular configurations shown in this work have all a zero Poisson's ratio behavior. ZPR is an essential mechanical parameter for span and chord length morphing, in particular for wing and rotary blade morphing. When combined with elastomeric of compliant matrices, they could be used as reinforcements for skins in span, chord length and camber adaptive applications [37,63]. The advantage of these TO-optimized ZPR cellular structures is the high specific transverse shear stiffness, that allows to increase the bending resistance of the skin, with no specific compromise on the in-plane compliance. The presence of the connecting plate at the end of the cell also allows an easier modular manufacturing of a skin with this particular type of reinforcement, as put in evidence by the demonstrator shown in Ref. [42].

6. Conclusions

The out-of-plane multi-stiffness topology optimization of the zero Poisson's ratio cellular structures for their applications in morphing skins has been presented in this work. The topology optimization has been performed using the combination of the popular SIMP method and the norm method with weighting coefficients. The optimized material distribution has been found meeting the requirement of both flatwise compressive and transverse shear stiffness, with a weight reduction of 31.77%. The topology optimization is the basis for the shape optimization and size optimization of the honeycomb design and could provide good guidance for designers to obtain an improved material distribution at the early design stage.
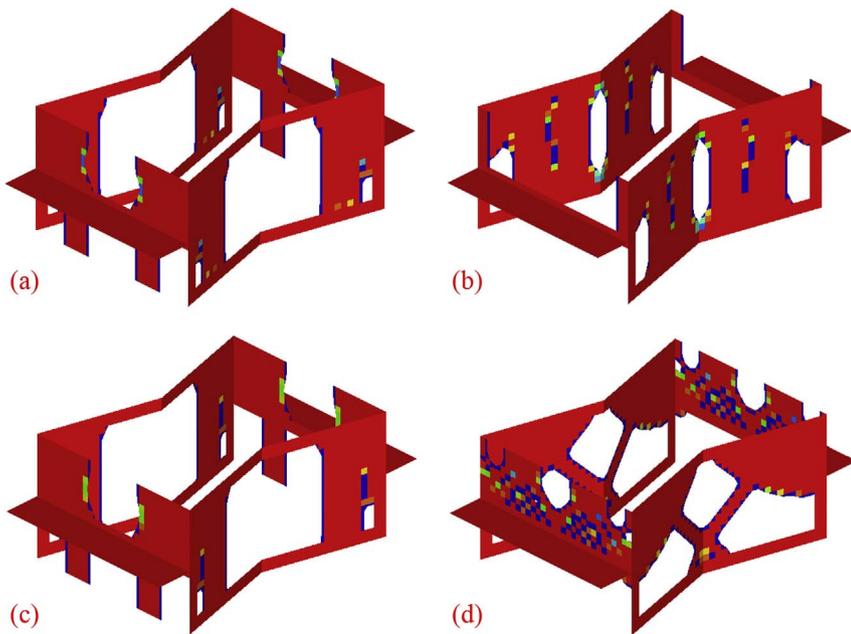
Fig. 11. Geometrical shape of the multi-stiffness topology optimization vs varying weighting coefficients: (a) $w_3 = 0.34$, $w_1 = w_2 = 0.33$; (b) $w_3 = w_1 = 0.5$, $w_2 = 0$; (c) $w_3 = w_2 = 0.5$, $w_1 = 0$; (d) $w_3 = 0$, $w_1 = w_2 = 0.5$.

References

[1] Gibson LJ, Ashby MF. Cellular solids: structure and properties. Cambridge university press; 1999.

[2] Bitzer T. Honeycomb technology: materials, design, manufacturing, applications and testing. Springer Science & Business Media; 2012.

[3] Liu L, Meng P, Wang H, Guan Z. The flatwise compressive properties of Nomex honeycomb core with debonding imperfections in the double cell wall. Compos B Eng 2015;76(Supplement C):122–32.

[4] Sun Z, Shi S, Guo X, Hu X, Chen H. On compressive properties of composite sandwich structures with grid reinforced honeycomb core. Compos B Eng 2016;94(Supplement C):245–52.

[5] Wang Z, Liu J, Hui D. Mechanical behaviors of inclined cell honeycomb structure subjected to compression. Compos B Eng 2017;110(Supplement C):307–14.

[6] Tao Y, Duan S, Wen W, Pei Y, Fang D. Enhanced out-of-plane crushing strength and energy absorption of in-plane graded honeycombs. Compos B Eng 2017;118(Supplement C):33–40.

[7] Choi W-H, Kim C-G. Broadband microwave-absorbing honeycomb structure with novel design concept. Compos B Eng 2015;83(Supplement C):14–20.

[8] Alderson A, Alderson KL, Chirima G, Ravirala N, Zied KM. The in-plane linear elastic constants and out-of-plane bending of 3-coordinated ligament and cylinder-ligament honeycombs. Compos Sci Technol 2010;70(7):1034–41.

[9] Evans KE. The design of doubly curved sandwich panels with honeycomb cores. Compos Struct 1991;17(2):95–111.

[10] Scarpa F, Tomlin PJ. On the transverse shear modulus of negative Poisson's ratio honeycomb structures. Fatig Fract Eng Mater Struct 2000;23(8):717–20.

[11] Bezazi A, Scarpa F, Remillat C. A novel centresymmetric honeycomb composite structure. Compos Struct 2005;71(3–4):356–64.

[12] Prall D, Lakes RS. Properties of a chiral honeycomb with a Poisson's ratio of -1. Int J Mech Sci 1997;39(3). 305-&.

[13] Miller W, Smith CW, Scarpa F, Evans KE. Flatwise buckling optimization of hexachiral and tetrachiral honeycombs. Compos Sci Technol 2010;70(7):1049–56.

[14] Lorato A, Innocenti P, Scarpa F, Alderson A, Alderson KL, Zied KM, et al. The transverse elastic properties of chiral honeycombs. Compos Sci Technol 2010;70(7):1057–63.

[15] Alderson A, Alderson KL, Attard D, Evans KE, Gatt R, Grima JN, et al. Elastic constants of 3-, 4-and 6-connected chiral and anti-chiral honeycombs subject to uniaxial in-plane loading. Compos Sci Technol 2010;70(7):1042–8.

[16] Chen YJ, Scarpa F, Liu YJ, Leng JS. Elasticity of anti-tetrachiral anisotropic lattices. Int J Solid Struct 2013;50(6):996–1004.

[17] Bacigalupo A, Gnecco G, Lepidi M, Gambarotta L. Optimal design of low-frequency band gaps in anti-tetrachiral lattice meta-materials. Compos B Eng 2017;115(Supplement C):341–59.

[18] Lakes R. Foam structures with a negative Poisson's ratio. Science 1987;235:1038–41.

[19] Evans KE, Alderson A. Auxetic materials: functional materials and structures from lateral thinking!. Adv Mater 2000;12(9). 617-+.

[20] Lim T-C. Auxetic materials and structures: Springer. 2014.

[21] Evans KE, Nkansah MA, Hutchinson IJ, Rogers SC. Molecular network design. Nature 1991;353(6340). 124-.

[22] Milton GW. Composite materials with Poisson's ratios close to -1. J Mech Phys Solid 1992;40(5):1105–37.

[23] Subramani P, Rana S, Ghiassi B, Fangueiro R, Oliveira DV, Lourenco PB, et al. Development and characterization of novel auxetic structures based on re-entrant hexagon design produced from braided composites. Compos B Eng 2016;93(Supplement C):132–42.

[24] Jin X, Wang Z, Ning J, Xiao G, Liu E, Shu X. Dynamic response of sandwich structures with graded auxetic honeycomb cores under blast loading. Compos B Eng 2016;106(Supplement C):206–17.

[25] Hou Y, Neville R, Scarpa F, Remillat C, Gu B, Ruzzene M. Graded conventional-auxetic Kirigami sandwich structures: flatwise compression and edgewise loading. Compos B Eng 2014;59(Supplement C):33–42.

[26] Mizzi L, Attard D, Gatt R, Pozniak AA, Wojciechowski KW, Grima JN. Influence of translational disorder on the mechanical properties of hexachiral honeycomb systems. Compos B Eng 2015;80(Supplement C):84–91.

[27] Chen Y, Scarpa F, Remillat C, Farrow I, Liu Y, Leng J. Curved Kirigami SILICOMB cellular structures with zero Poisson's ratio for large deformations and morphing. J Intell Mater Syst Struct 2014;25(6):731–43.

[28] Lira C, Scarpa F, Olszewska M, Celuch M. The SILICOMB cellular structure: mechanical and dielectric properties. Phys Status Solidi B-Basic Solid State Phys 2009;246(9):2055–62.

[29] Lira C, Scarpa F, Tai YH, Yates JR. Transverse shear modulus of SILICOMB cellular structures. Compos Sci Technol 2011;71(9):1236–41.

[30] Virk K, Monti A, Trehard T, Marsh M, Hazra K, Boba K, et al. SILICOMB PEEK Kirigami cellular structures: mechanical response and energy dissipation through zero and negative stiffness. Smart Mater Struct 2013;22(8).

[31] Grima JN, Oliveri L, Attard D, Ellul B, Gatt R, Cicala G, et al. Hexagonal honeycombs with zero Poisson's ratios and enhanced stiffness. Adv Eng Mater 2010;12(9):855–62.

[32] Grima JN, Attard D. Molecular networks with a near zero Poisson's ratio. Phys Status Solidi B-Basic Solid State Phys 2011;248(1):111–6.

[33] Attard D, Grima JN. Modelling of hexagonal honeycombs exhibiting zero Poisson's ratio. Phys Status Solidi B-Basic Solid State Phys 2011;248(1):52–9.

[34] Olympio KR, Gandhi F. Zero Poisson's ratio cellular honeycombs for flex skins undergoing one-dimensional morphing. J Intell Mater Syst Struct 2009;21(17):1737–53.

[35] Neville RM, Monti A, Hazra K, Scarpa F, Remillat C, Farrow IR. Transverse stiffness and strength of Kirigami zero-nu PEEK honeycombs. Compos Struct 2014;114:30–40.

[36] Bubert EA, Woods BK, Lee K, Kothera CS, Wereley NM. Design and fabrication of a passive 1D morphing aircraft skin. J Intell Mater Syst Struct 2010;21(17):1699–717.

[37] Olympio KR, Gandhi F. Flexible skins for morphing aircraft using cellular honeycomb cores. J Intell Mater Syst Struct 2010;21(17):1719–35.

[38] Engelmayr Jr. GC, Cheng M, Bettinger CJ, Borenstein JT, Langer R, Freed LE. Accordion-like honeycombs for tissue engineering of cardiac anisotropy. Nat Mater 2008;7(12):1003–10.

[39] Huang J, Gong X, Zhang Q, Scarpa F, Liu Y, Leng J. In-plane mechanics of a novel zero Poisson's ratio honeycomb core. Compos B Eng 2016;89:67–76.

[40] Huang J, Zhang Q, Scarpa F, Liu Y, Leng J. In-plane elasticity of a novel auxetic

honeycomb design. Compos B Eng 2017;110:72–82.

[41] Huang J, Zhang Q, Scarpa F, Liu Y, Leng J. Bending and benchmark of zero Poisson's ratio cellular structures. Compos Struct 2016;152:729–36.

[42] Huang J, Zhang Q, Scarpa F, Liu Y, Leng J. Shape memory polymer-based hybrid honeycomb structures with zero Poisson's ratio and variable stiffness. Compos Struct 2017;179:437–43.

[43] Boucher MA, Smith CW, Scarpa F, Rajasekaran R, Evans KE. Effective topologies for vibration damping inserts in honeycomb structures. Compos Struct 2013;106:1–14.

[44] Strek T, Jopek H, Idczak E. Computational design of two-phase auxetic structures. Phys Status Solidi 2016;253(7):1387–94.

[45] Eschenauer HA, Olhoff N. Topology optimization of continuum structures: a review. Appl Mech Rev 2001;54(4):331–90.

[46] Bremicker M, Chirehdast M, Kikuchi N, Papalambros PY. Integrated topology and shape optimization in structural design. Mech Struct Mach 1991;19(4):551–87.

[47] Olhoff N, Bendsoe MP, Rasmussen J. On CAD-integrated structural topology and design optimization. Comput Meth Appl Mech Eng 1991;89(1–3):259–79.

[48] Bendsoe MP, Kikuchi N. Generating optimal topologies in structural design using a homogenization method. Comput Meth Appl Mech Eng 1988;71(2):197–224.

[49] Bendsøe MP. Optimal shape design as a material distribution problem. Struct Multidiscip Optim 1989;1(4):193–202.

[50] Zhou M, Rozvany GIN. The COC algorithm, Part II: topological, geometrical and generalized shape optimization. Comput Meth Appl Mech Eng 1991;89(1–3):309–36.

[51] Rozvany GIN, Zhou M, Birker T. Generalized shape optimization without homogenization. Struct Optim 1992;4(3–4):250–2.

[52] Xie YM, Steven GP. A simple evolutionary procedure for structural optimization. Comput Struct 1993;49(5):885–96.

[53] Sethian JA, Wiegmann A. Structural boundary design via level set and immersed interface methods. J Comput Phys 2000;163(2):489–528.

[54] Wang MY, Chen SK, Wang XM, Mel YL. Design of multimaterial compliant mechanisms using level-set methods. J Mech Des 2005;127(5):941–56.

[55] Allaire G, Jouve F, Toader AM. Structural optimization using sensitivity analysis and a level-set method. J Comput Phys 2004;194(1):363–93.

[56] Bourdin B, Chambolle A. Design-dependent loads in topology optimization. ESAIM Control, Optim Calc Var 2003;9(2):19–48.

[57] Eschenauer HA, Kobelev VV, Schumacher A. Bubble method for topology and shape optimization of structures. Struct Optim 1994;8(1):42–51.

[58] Sokolowski J, Zochowski A. On the topological derivative in shape optimization. SIAM J Contr Optim 1999;37(4):1251–72.

[59] Gong X, Huang J, Scarpa F, Liu Y, Leng J. Zero Poisson's ratio cellular structure for two-dimensional morphing applications. Compos Struct 2015;134:384–92.

[60] Min S, Nishiwaki S, Kikuchi N. Unified topology design of static and vibrating structures using multiobjective optimization. Comput Struct 2000;75(1):93–116.

[61] Koski J, Silvennoinen R. Norm methods and partial weighting in multicriterion optimization of structures. Int J Numer Meth Eng 1987;24(6):1101–21.

[62] Chen TY, Wu SC. Multiobjective optimal topology design of structures. Comput Mech 1998;21(6):483–92.

[63] Olympio KR, Gandhi F. Zero Poisson's ratio cellular honeycombs for flex skins undergoing one-dimensional morphing. J Intell Mater Syst Struct 2010;21(17):1737–53.